Journal of Radioanalytical Chemistry, Vol. 76, No. 1 (1983) 151–170

DETERMINATION OF REACTOR NEUTRON SPECTRA WITH MULTICOMPONENT ACTIVATION DETECTORS

J. V. SANDBERG,* P. D. LUND

Helsinki University of Technology
Department of Technical Physics,
SF–02150 Espoo 15 (Finland)

(Received January 18, 1982)

A procedure is described for the functional fitting of reactor neutron spectra with C/E^n and fission spectra. The method is applied to multicomponent activation detector measurements in a Triga research reactor. In multicomponent detectors a mixture of several detector materials is irradiated as a single unit and measured simultaneously for all reaction products with a Ge(Li) gamma ray spectrometer.

Introduction

Activation detectors are commonly used for measuring neutron energy spectra. To make spectrum measurements simpler and faster Multicomponent Activation Detectors (MAD) have been developed recently.[1-3] In this paper we report a simple method for the least-squares functional fitting of fast and intermediate reactor neturon spectra with an application to multicomponent detector measurements.

In conventional activation detector spectrum measurements, a package of several detector foils or wires of different materials is irradiated. Afterwards the foils are taken apart and measured separately, generally for gamma active reaction products and their saturation activities are determined. The neutron spectrum can be determined with the measured activities using functional fitting or unfolding programs.

The principle of a MAD is to use a mixture of several detector materials and to measure all product nuclides with a single gamma spectrum measurement. The advantages of MADs are the possibility to produce cheaply large numbers of small, standardized detectors, as well as the reduced number of gamma spectrum measurements. Separate multicomponent resonance and threshold detectors have been designed for intermediate and fast neutrons. The selection of detector reactions, the optimization of the masses and irradiation, waiting and measuring times and the fabrication of the detectors are described in Refs.[1,3]

MADs can be optimized for various types of neutron spectra. Here we consider resonance and threshold reaction detectors designed for a thermal Triga research

*Author to whom all correspondence should be addressed.

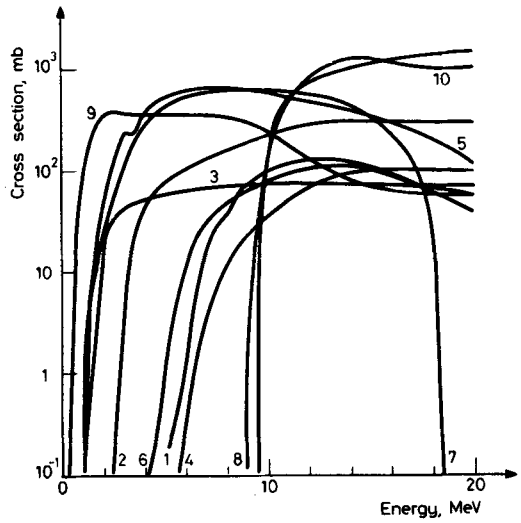

Fig. 1. Threshold reaction cross-sections.[19] The niobium cross-section includes both g and m states and it is assumed that 44.4% of ^{92}Nb is produced in the m state.[9]
Curves: 1 = ^{27}Al (n, α) ^{24}Na, 2 = ^{46}Ti (n, p) ^{46}Sc, 3 = ^{47}Ti (n, p) ^{47}Sc, 4 = ^{48}Ti (n, p) ^{48}Sc, 5 = ^{54}Fe (n, p) ^{54}Mn, 6 = ^{56}Fe (n, p) ^{56}Mn, 7 = ^{58}Ni (n, p) ^{58}Co, 8 = ^{93}Nb (n, 2n) ^{92}Nb, 9 = ^{115}In (n, n') ^{115m}In, 10 = ^{127}I (n, 2n) ^{126}I

reactor. The composition of the detectors and nuclear properties of the components are given in Tables 1 and 2. Cross-sections of threshold reactions are shown in Fig. 1. The detectors are ancapsulated in quartz glass ampoules with inner diameters of 0.5 cm and length of 5.5 cm. When the irradiation temperature allows, also polyethylene capsules can be used. The resonance detector is made by evaporating solutions of detector materials in the ampoule. In the threshold detector, an indium solution is evaporated and the other components are added as powders or pieces of metal wires. The detectors are surrounded with cadmium shields to exclude thermal activation.

The neutron spectrum, which is searched after, can be unfolded from the detector activities by solving the integral equations

$$A_i = \int_{E_{min}}^{E_{max}} \sigma_i(E)\,\phi(E)\,dE, \quad i = 1, \ldots, m \qquad (1)$$

where A_i = measured saturation activity of detector i, normalized per one detector nucleus,
$\sigma_i(E)$ = cross section of detector i,
$\phi(E)$ = flux spectrum to be solved,
m = number of detector components.

Table 1
Composition and nuclear properties[9,14,20,21] of a multicomponent resonance detector for Triga reactor. The optimized irradiation time is 150 min, waiting time 35 min and measuring time 120 min

Reaction	Resonance energy, eV	Resonance integral I', barn	σ_0, barn	Half-life	γ-energy used in this work, keV	Branching ratio, %	Isotope fraction in natural element, %	Mass of natural element, μg
^{115}In (n, γ) ^{116m}In	1.46	2440	160.0	54.3 m	1097.	55.7	95.72	0.4
^{197}Au (n, γ) ^{198}Au	4.906	1490	98.8	64.7 h	411.8	95.5	100.	2.0
^{186}W (n, γ) ^{187}W	18.8	486	34.0	23.9 h	479.5	26.6	28.9	27.4
^{75}As (n, γ) ^{76}As	47	58.0	5.4	26.4 h	559.1	44.6	100	25.2
^{198}Pt (n, γ) ^{199}Pt	95	48.1	3.7	31.0 m	317.	5.6	7.21	1016.0
^{55}Mn (n, γ) ^{56}Mn	337	9.4	13.3	2.58 h	846.6	99.0	100.	6.0
^{63}Cu (n, γ) ^{64}Cu	580	3.17	4.51	12.7 h	511.	37.0	69.1	165.
^{23}Na (n, γ) ^{24}Na	2850	0.075	0.525	15.0 h	1368.6	100.	100.	352.

Table 2
Composition and nuclear properties[19-21] of a multicomponent threshold detector
for Triga reactor. The optimized irradiation time is 180 min, waiting time 960 min and measuring time 180 min

Reaction	Threshold energy, MeV	σ_{eff}, mb	Half-life	γ-energy used in this work, keV	Branching ratio, %	Isotope fraction in natural element, %	Natural element mass, mg
^{27}Al (n, α) ^{24}Na	7.0	49.7	15.0 h	1368.5	100.	100.	10.0
^{46}Ti (n, p) ^{46}Sc	4.0	107	84.2 d	889.3	100.	7.99	145.
^{47}Ti (n, p) ^{47}Sc	2.2	48.8	3.4 d	159.4	70.	7.32	145.
^{48}Ti (n, p) ^{48}Sc	7.6	30.1	1.84 d	983.5	100.	73.99	145.
^{54}Fe (n, p) ^{54}Mn	3.3	404.	313 d	834.8	100.	5.89	200.
^{56}Fe (n, p) ^{56}Mn	6.1	42.5	2.58 h	846.7	99.	91.68	200.
^{58}Ni (n, p) ^{58}Co	2.8	470	71.3 d	810.6	99.4	67.76	50.
^{93}Nb (n, 2n) ^{92m}Nb	10.2	317	10.2 d	934.5	99.	100	150.
^{115}In (n, n') ^{115m}In	1.3	294	4.48 h	336.3	44.5	95.77	1.

The flux cannot be solved uniquely from Eq. (1) without some prior information on the solution. In the present method the neutron spectrum is determined by fitting parameters in predetermined equations. Several more sophisticated unfolding programs with better resolution, such as LOUHI,[4] SAND II[5] and STAY'SL,[6] can also be used, but in many cases functional fitting is sufficient.

The methods described here have been implemented in the Multicomponent Activation Detector Analysis Program (MADAP), which has been installed on a UNIVAC 1108 large scale computer and on a NOVA 2 minicomputer with a 32 kword core memory.[7]

Saturation activities

Gamma spectrum analysis

For the determination of gamma peak counts and saturation activities we use the gamma spectrum analysis and nuclide identification program SAMPO80,[8] which is installed on our minicomputer. In SAMPO80, gamma peak search is based on a second derivative method and the peak counts are determined by fitting precalibrated Gaussian functions with exponential tails to the peaks and integrating the fitted function.

When the gamma peak counts have been determined, the saturation activities can be calculated as

$$A_i' = \lambda_i N_i / (f_i b_i (1-e^{-\lambda_i t_1}) e^{-\lambda_i t_2} (1-e^{-\lambda_i t_3}) K_i) \qquad (2)$$

where N_i – gamma peak area,
K_i – number of atoms of the detector nuclide,
f_i – γ counting efficiency,
b_i – branching ratio of the peak,
λ_j – decay constant,
t_1 – activation time,
t_2 – waiting time,
t_3 – counting time.

If a nuclide can be produced either directly in the ground state or through a metastable isometric state, the effect of the isomeric state on the activity determination should be checked. In our multicomponent detectors the only disturbing isomeric state is ^{58m}Co with about 31.3% yield in reaction ^{58}Ni (n, p) ^{58}Co.[9] The half-lives of the isomeric state and the ground state are 9.15 h and 71.3 d, respectively, and in our case a 7% correction was required in the saturation activity.

Since the MADs have been optimized to give gamma spectra with well distinguishable peaks,[1,3] less sophisticated gamma spectrum analysis methods than

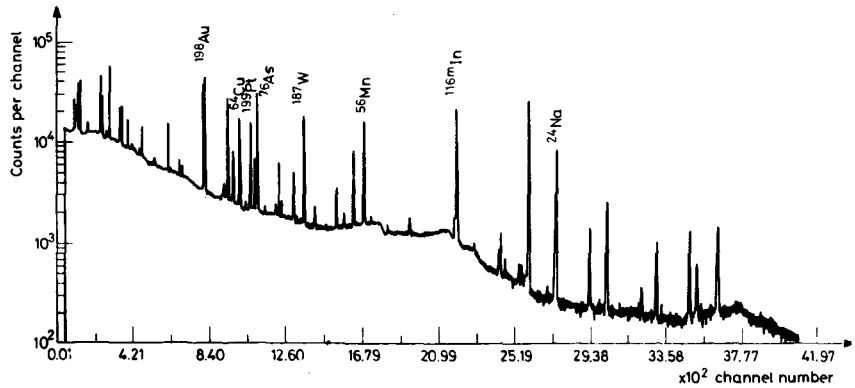

Fig. 2. A gamma spectrum of an optimized multicomponent resonance detector

SAMPO are also adequate. We have coded a subroutine in MADAP for computing peak counts with simple summation and linear background subtraction. In practice the absolute difference of peak counts as compared to SAMPO80 is about 6% on the average with largest deviations about 15%.[7] A typical 4096 channel gamma spectrum of a resonance detector is shown in Fig. 2. Spectra of threshold detectors are of comparable complexity.

Self-shielding and impurity corrections

The saturation activities A_i corresponding to the unperturbed flux are related to the measured saturation activities A_i' given by Eq. (2), through the relation

$$A_i = \int_{E_{min}}^{E_{max}} \sigma(E)\,\phi(E)\,dE = \frac{1}{G_i} A_i' \tag{3}$$

The correction factor G_i involves three components

$$G_i = S_i R_i P_i \tag{4}$$

where S_i is the self-shielding correction factor, which accounts for the absorption of neutrons in the detector, R_i accounts for the absorption of γ-rays of product nuclides in the detector and P_i is an impurity correction.

The self-shielding correction S_i of resonance detectors can be estimated assuming that the mass is distributed as a thin layer on the bottom of the ampoule with a dia-

Table 3
Correction factors for multicomponent resonance detectors in quartz ampoules

Reaction	Self-shielding correction S_i	γ-ray attenuation correction R_i	Impurity correction P_i	Total correction factor G_i
$^{115}In\ (n, \gamma)\ ^{116}In$	0.998	0.987	1.	0.985
$^{197}Au\ (n, \gamma)\ ^{198}Au$	0.993	0.979	1.	0.972
$^{186}W\ (n, \gamma)\ ^{187}W$	0.999	0.981	1.	0.980
$^{75}As\ (n, \gamma)\ ^{76}As$	0.981	0.982	1.	0.963
$^{198}Pt\ (n, \gamma)\ ^{199}Pt$	0.873	0.978	1.	0.854
$^{55}Mn\ (n, \gamma)\ ^{56}Mn$	0.994	0.986	1.022	1.002
$^{63}Cu\ (n, \gamma)\ ^{64}Cu$	0.950	0.981	1.016	0.947
$^{23}Na\ (n, \gamma)\ ^{24}Na$	0.906	0.987	1.028	0.919

meter of 0.2 cm. We can, therefore, use an equation derived for an infinite planar detector[10]

$$S_i = \frac{1}{\sqrt{1 + 2n_i\sigma_{ot,i}\,\delta}}, \tag{5}$$

where n_i – atomic density of component i,
$\sigma_{ot,i}$ – maximum value of the total cross section at the resonance peak,
δ – thickness of the detector.

Numerical values of correction factors are given in Table 3. The values which deviate most from unity belong to resonances with large scattering components. The scattering removes neutrons from the resonance energy without contribution to activation. The self-shielding correction is close to unity if the resonance involves mainly neutron capture and if the product nuclide has a moderate half-life so that sufficient activity can be produced in a small mass. Small self-shielding effects are desirable because the estimation of the correction involves errors e. g. due to the uncertainty of the thickness of the detector.

The attenuation of gamma-rays in the detector materials is negligible but some attenuation is caused by the quartz ampoule. The impurity corrections P_i were determined by activation analysis of detector and ampoule materials for possibly interfering reaction products. The only significant impurities were 4.86 ppm sodium and 0.065 ppm manganese in quartz glass. ^{64}Cu was determined using the 511 keV β^+ annihilation peak. Annihilation radiation is produced also through pair production and successive annihilation in the Ge(Li) detector. The pair production was caused mainly by the 2754 keV peak of ^{24}Na. The contribution was determined

experimentally and it was found that a 1.6% reduction had to be made in the ^{64}Cu activity.

The estimation of neutron self-shielding for threshold detectors is more complicated that for resonance detectors. In threshold detectors all reactions occurring in any component over a wide energy range should be considered, whereas in resonance detectors the self-shielding is concentrated at the resonance energies which are specific to each component. We estimate the order of magnitude of the self-shielding correction by considering ^{93}Nb which has by far the largest cross-section of the components,715 mb. If we assume that the niobium is distributed in a sphere with radius r and solid Nb density, which is a worst case assumption, the self-shielding correction can be estimated as[10,11]

$$S = 1 - \frac{3}{4} r \Sigma_a, \tag{6}$$

where Σ_a is the macroscopic absorption cross-section. With r = 0.16 cm we get $S \approx 0.995$. As the cross-sections of the other reactions are much smaller and the other masses are of the same order of magnitude or smaller, we conclude that the self-shielding corrections are about 0.5% or less, which we consider negligible and we set $S_i = 1$ for all threshold reactions.

In threshold detectors the attenuation of gamma rays in the detector materials must be taken into account. If we assume that the component materials are distributed homogeneously in a detector cylinder with height H = 0.5 cm and radius R = 0.25 cm, we get the following expression for the average attenuation coefficient for each γ energy

$$\mu_i = \sum_{j=1}^{k} \frac{m_i}{V} \left(\frac{\mu}{\rho}\right)_i, \quad i = 1, \ldots, k \tag{7}$$

where m_i – mass of component i,

$\left(\frac{\mu}{\rho}\right)_i$ – mass attenuation coefficient of component i, given in Ref.[12],

$V = \pi R^2 H$ – volume of the detector.

When the detectors are counted with the bottom towards the Ge(Li) detector, the attenuation correction can be estimated by one-dimensional calculation as

$$R_i = (1 - e^{-\mu_i H}) / \mu_i H. \tag{8}$$

The small correction caused by the quartz ampoule was also taken into account. For indium, which was evaporated on the bottom of the ampoule only the attenuation of the ampoule wall was considered. A correction was also made for the Na and Mn impurities present in quartz. The correction factors are given in Table 4.

Table 4
Correction factors for multicomponent threshold detectors in quartz ampoules

Reaction	Self-shielding correction S_i	γ-ray attenuation correction R_i	Impurity cirrection P_i	Total correction factor G_i
$^{27}Al\ (n, \alpha)\ ^{24}Na$	1.	0.922	1.115	1.028
$^{46}Ti\ (n, p)\ ^{46}Sc$	1.	0.904	1.	0.904
$^{47}Ti\ (n, p)\ ^{47}Sc$	1.	0.730	1.	0.730
$^{48}Ti\ (n, p)\ ^{48}Sc$	1.	0.909	1.	0.909
$^{54}Fe\ (n, p)\ ^{54}Mn$	1.	0.901	1.	0.901
$^{56}Fe\ (n, p)\ ^{56}Mn$	1.	0.902	1.002	0.903
$^{58}Ni\ (n, p)\ ^{58}Co$	1.	0.900	1.	0.900
$^{93}Nb\ (n, 2n)\ ^{92m}Nb$	1.	0.907	1.	0.907
$^{115}In\ (n, n')\ ^{115m}In$	1.	0.981	1.	0.981

The cadmium cover of the detectors used to exclude thermal neutrons causes some attenuation in the epithermal flux, too. This effect is usually small and is difficult to determine accurately, but we estimate that in our measurements the effect is about one per cent. Since the effect is common to all epithermal activation detectors and not a property of the MAD, it is not treated here in detail.

Neutron spectrum fitting

Intermediate spectrum

The intermediate neutron spectrum is fitted in the least squares sense to the equation

$$\phi(E) = C/E^n \tag{9}$$

where E is the neutron energy and C and n are parameters to be determined.[13] The intermediate neutron flux in an infinite hydrogen moderator can be theoretically shown to follow Eq. (9) with n = 1. Absorption and the finite size of the reactor can be largely taken into account by changing the parameter n. Note that in Eq. (9) E should be divided by the energy unit to get the dimensions consistent, but for simplicity of notation this is not done explicitly.

To avoid thermal activation, the detectors are irradiated in cadmium boxes, and the activation is caused by neutrons with energies above the effective cadmium cut-off energy E_{Cd}. The cut-off energy depends on the thickness of the Cd-cover, for a 1 mm thick cover $E_{Cd} \approx 0.55$ eV.[14]

Suppose that a resonance detector has a narrow resonance at energy $E_{r,i}$ with resonance integral I_i' and a cross-section of 1/v-type

$$\sigma_{1/v,i} = \sigma_{o,i}\sqrt{E_o/E} \tag{10}$$

where $\sigma_{o,i}$ is the cross section at energy $E_o = 0.0253$ eV.

The saturation activity per one detector atom of Cd-covered detector i with resonance energy $E_{r,i}$ is

$$A_i = \int_{E_{Cd}}^{\infty} \sigma_i(E)\frac{C}{E^n}\,dE$$

$$\approx C[E_{r,i}^{1-n} I_i' + I_{1/v,i}(n)] = A_{res,i} + A_{1/v,i}, \tag{11}$$

where

$$I_{1/v,i}(n) = \int_{E_{Cd}}^{\infty} \sigma_{1/v,i}(E)\frac{dE}{E^n} = \sigma_{o,i}E_o^{1/2}E_{Cd}^{1/2-n}/(n-1/2) \tag{12}$$

and I_i' is the resonance integral, 1/v-contribution excluded[10]

$$I_i' = \int_{E_{Cd}}^{\infty} \frac{1}{E}\sigma_{res,i}(E)\,dE \tag{13}$$

If we denote

$$T_i(n) = \frac{A_{res,i}}{A_{i,res} + A_{1/v,i}} = \frac{E_{r,i}^{1-n} I_i'}{E_{r,i}^{1-n} I_i' + I_{1/v,i}(n)} \tag{14}$$

we have

$$A_{res,i} = C\,E_{r,i}^{1-n} I_i' = T_i(n) A_i. \tag{15}$$

The parameters C and n can be determined using least-squares fitting iteratively. First it is supposed that n = 1. Eq. (15) can then be used to solve $C = C_i(n)$ for each detector component, since A_i is known and $T_i(n)$ can be calculated if n is fixed. Thus the neutron flux at each resonance energy is

$$\phi_i = C_i(n)/E_{r,i}^n, \tag{16}$$

where n = 1 for the first iteration step. On a log-log scale the flux of Eq. (9) is a straight line with slope -n

$$\ln \phi(E) = \ln C - n \ln E. \tag{17}$$

The data points ($\ln E_{r,i}$, $\ln \phi_i$), $i = 1, ..., m$,
where

$$\phi_i = T_i(n)\, A_i / (E_{r,i}\, I_i'), \tag{18}$$

are fitted to Eq. (17) using an iterative least-squares technique.

The problem can be posed as an overdetermined system of linear equations for ln C and n

$$\ln \phi_i = \ln C - n \ln E_{r,i} + \epsilon_i, \quad i = 1, ..., m. \tag{19}$$

This problem can be solved by linear estimation theory. First we have to estimate the variance matrix of $\ln \phi_i$.

The statistical uncertainty in ϕ_i is caused by the uncertainty in the saturation activity and in the cross section data. The uncertainty can be approximated as

$$\Delta \phi_i = \sqrt{\left(\frac{\partial \phi_i}{\partial A_i}\, \Delta A_i\right)^2 + \left(\frac{\partial \phi_i}{\partial I_i'}\, \Delta I_i'\right)^2} \tag{20}$$

$$= \phi_i \sqrt{\left(\frac{\Delta A_i}{A_i}\right)^2 + \left(T_i(n)\, \frac{\Delta I_i'}{I_i'}\right)^2} \tag{21}$$

The error in the 1/v-cross-section is not considered, because its contribution is usually small compared to that of the resonance integral. The uncertainty of $\ln \phi_i$ is

$$\Delta \ln \phi_i \approx \frac{\partial \ln \phi_i}{\partial \phi_i}\, \Delta \phi_i = \Delta \phi_i / \phi_i, \quad i = 1, ..., m, \tag{22}$$

The variance matrix $\alpha^2 \underline{V}$ of $\ln \phi_i$'s can be assumed diagonal with the elements[15,16]

$$\alpha^2 V_{ii} = \Delta \phi_i / \phi_i, \quad i = 1, ..., m, \tag{23}$$

where α^2 is so far an undetermined constant.

Let us denote

$$\underline{X} = \begin{bmatrix} \ln C \\ n \end{bmatrix} \qquad \underline{K} = \begin{bmatrix} 1 & -\ln E_{r,1} \\ \vdots & \\ 1 & -\ln E_{r,m} \end{bmatrix} \qquad \underline{Y} = \begin{bmatrix} \ln \phi_1 \\ \cdot \\ \vdots \\ \ln \phi_m \end{bmatrix} \tag{24}$$

where ϕ_i is calculated with Eq. (18) for each iteration step with n.

Eqs (19) can now be expressed in matrix form as

$$\underline{Y} = \underline{K}\,\underline{X} + \underline{\epsilon} \tag{25}$$

where $\underline{\epsilon}$ is a normally distributed error vector with zero mean values and a diagonal variance matrix $\alpha^2 \underline{V}$. The miniumum norm solution of Eq. (25) is obtained by minimizing the square sum Q

$$Q = (\underline{Y} - \underline{K}\,\underline{X})^T (\alpha^2\,\underline{V})^{-1} (\underline{Y} - \underline{K}\,\underline{X}) \tag{26}$$

The solution is[15,16]

$$\underline{X} = (\underline{K}^T \underline{V}^{-1}\,\underline{K})^{-1}\,\underline{K}^T \underline{V}^{-1}\,\underline{Y} \tag{27}$$

with the variance matrix

$$\underline{\Sigma} = \alpha^2\,(K^T \underline{V}^{-1}\,\underline{K})^{-1} \tag{28}$$

Thus we get the following parameter values and their error estimates

$$C = e^{X_1}$$

$$\Delta C = C\Delta(\ln C) = C\sqrt{\Sigma_{11}} \tag{29}$$

$$n = X_2$$

$$\Delta n = \sqrt{\Sigma_{22}} \tag{30}$$

Note that the solution does not depend on the normalizing constant α^2 of the variance matrix, whereas the error extimate does. The constant α^2 can be fixed as follows. The estimate of the square sum Q in Eq. (26) can be shown to be[16]

$$\hat{Q} = (m - 2)\,\alpha^2 \tag{31}$$

where $m - 2$ is the degree of freedom of the problem with m detectors and two unknown parameters. On the other hand, the actual Q can be calculated at the minimum point. When we set $\hat{Q} = Q$ we get

$$\alpha^2 = Q/(m-2) \tag{32}$$

The fitted value of n can be used to calculate new values for T_i (n), i = 1, ..., m, in Eq. (14). The least-squares procedure is then repeated until convergence of C and n is reached.

When the parameters C and n with their error estimates ΔC and Δn have been determined, the flux and its confidence band can be calculated as

$$\phi\,(E) = C/E^n \tag{33}$$

$$|\Delta\phi\,(E)| = \sqrt{\left(\frac{\Delta C}{E^n}\right)^2 + \left(\frac{C\ \ell n\, E\, \Delta n}{E^n}\right)^2} \tag{34}$$

These expressions are valid with reasonable accuracy above the cadmium cut-off energy up to about 0.5 MeV in a thermal reactor.

Fast neutron spectrum

In the MeV region the reactor spectrum is approximately equal to the fission neutron spectrum. Several empirical equations of the fission spectrum with one to three free parameters have been suggested.[14,17] Here we use the equation

$$\phi\,(E) = a\, e^{-bE}\, \sinh\sqrt{2\,E}\,, \tag{35}$$

where E is the neutron energy in MeV and a and b are parameters to be fitted. With b = 1, Eq. (35) is the WATT fission spectrum.[17] We have optionally used b as a free parameter so that the slope of the spectrum is determined by the measured data.

Let us assume that the fitting errors have the variances $\beta^2\, V_{ii}$, where β^2 is so far an unknown constant,

$$V_{ii} = (\Delta A_i)^2 = (A_i^m)^2 \left[\left(\frac{\Delta N_i}{N_i}\right)^2 + \left(\frac{\Delta\sigma_i}{\sigma_i}\right)^2\right], \quad i = 1, \ldots, k, \tag{36}$$

where A_i^m – measured saturation activity,

$\Delta N_i/N$ – relative error of peak count,

$\Delta\sigma_i/\sigma_i$ – energy-averaged uncertainty of section i,

k – number of threshold reactions.

Special weights can also be included in V_{ii}.

The parameters a and b can then be determined by minimizing the square sum[15,16]

$$Q = \sum_{i=1}^{k} \frac{1}{\beta^2\, V_{ii}}\, [A_i^m - A_i^c\,(a, b)]^2 \tag{37}$$

where

$$A_i^c = \int_{E_{min}}^{E_{max}} \sigma_i\,(E)\, \phi\,(a,b;E)\, dE, \quad i = 1, \ldots, k, \tag{38}$$

are the calculated saturation activities.

For numerical solution the integration must be replaced by summation

$$A_i^c(a,b) = a \sum_{j=1} W_j \sigma_{ij} e^{-bE_j} \sin h\sqrt{2E_j} = a A_i^* \tag{39}$$

where $W_j, j = 1, ..., n$ are quadrature weights.

The minimization of Q is done as a two-step procedure. When b is fixed, the normalization factor a can be expressed as

$$a = \frac{\sum_{i=k}^{k} A_i^m A_i^* V_{ii}}{\sum_{i=1}^{k} (A_i^*)^2 V_{ii}} \tag{40}$$

Q is minimized by iteration with respect to b. First b is set equal to $b_0 = 1$, and the corresponding equation is solved. The direction where Q decreases is determined by calculating Q at b_0 and $b_0 \pm \delta$. Next, b is set equal to $b + \Delta b$ and the same procedure is carried out iteratively halving the change in b at each step until a minimum is found.

If $e^{-Q/2}$ is interpreted as a joint probability density of parameters a and b, their variances (and error estimates) can be constructed using the Hessian or second derivatives matrix.[18]

Let us first calculate the derivatives of $A_i^c(a, b)$

$$\frac{\partial A_i^c(a,b)}{\partial a} = \sum_j \sigma_{ij} W_j e^{-bE_j} \sinh\sqrt{2E_j} = \frac{1}{a} A_i^c(a,b) \tag{41}$$

$$\frac{\partial^2 A_i^c}{\partial a^2} = 0 \tag{42}$$

$$\frac{\partial A_i^c(a,b)}{\partial b} = -\sum_{j=1}^{n} \sigma_{ij} W_j E_j \phi(E_j) \tag{43}$$

$$\frac{\partial^2 A_i^c(a,b)}{\partial b^2} = \sum_{j=1}^{n} \sigma_{ij} W_j E_j^2 \phi(E_j) \tag{44}$$

The elements of the Hessian matrix are then

$$H_{11} = \frac{\partial^2 Q}{\partial a^2} = +2 \sum_{i=1}^{k} \frac{1}{\beta^2 V_{ii}} \left[\frac{A_i^c(a,b)}{a}\right]^2 \tag{45}$$

$$H_{12} = \frac{\partial^2 Q}{\partial a \partial b} = -2 \sum_{i=1}^{k} \frac{1}{\beta^2 V_{ii}} (A^m_i - 2A^c_i) \frac{1}{a} \frac{\partial A^c_i}{\partial b} \tag{46}$$

$$H_{22} = \frac{\partial^2 Q}{\partial b^2} = -2 \sum_{i=1}^{k} \frac{1}{\beta^2 V_{ii}} (A^m_i - A^c_i) \frac{\partial^2 A^c_i}{\partial b^2} \tag{47}$$

$$+ 2 \sum_{i=1}^{k} \frac{1}{\beta^2 V} \left[\frac{\partial A^c_i}{\partial b} \right]^2$$

The standard deviations of a and b, which can be used as their error estimates, can be constructed using the diagonal elements of the inverse of the Hessian matrix

$$\Delta a = \sqrt{(H^{-1})_{11}}$$
$$\Delta b = \sqrt{(H^{-1})_{22}} \,. \tag{48}$$

The parameter β^2 can be determined by equating the estimated value

$$\hat{Q} = (k-2)\beta^2 \tag{49}$$

with the actual value of Q, which gives

$$\beta^2 = Q/(k-2). \tag{50}$$

When a and b and their error estimates have been determined, the spectrum can be calculated from Eq. (35) and the error estimate for the spectrum is

$$|\Delta\phi(E)| = \sqrt{\Delta a^2 + (ab\Delta b)^2}\; e^{-bE} \sinh\sqrt{2E} \tag{51}$$

These equations are used above 0.5 MeV.

Applications

Measured spectra in a Triga reactor

As an application of the methods described above we consider the determination of the fast and intermediate spectra in our 250 kW Triga research reactor. The measurements were carried out in the irradiation position in the core of the reactor using the optimized threshold and resonance detectors. The parameters fitted by the program

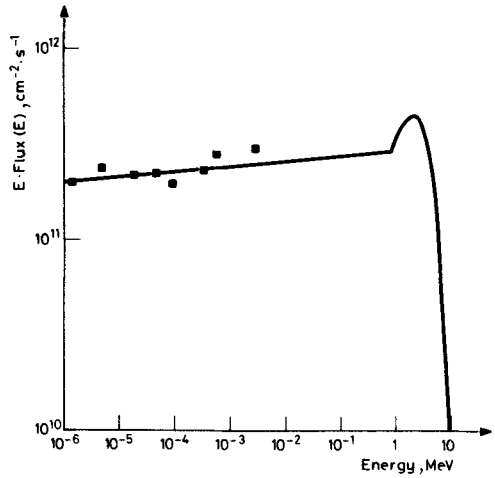

Fig. 3. Epithermal neutron flux spectrum in a 250 kW Triga research reactor. The squares mark flux values calculated with single resonance detectors. The corresponding saturation activities are given in Tables 6 and 7.

Table 5
Fitted parameters of the intermediate spectrum, Eq. (9), and fission spectrum, Eq. (35), corresponding to the Triga reactor spectrum shown in Fig. 3

$C = 2.04 \cdot 10^{11} \pm 3.6 \cdot 10^{9}$ $n \cdot cm^{-2} \cdot s^{-1} \cdot eV^{-1}$

$n = 0.974 \pm 0.080$

$a = 4.373 \cdot 10^{5} \pm 8.9 \cdot 10^{3}$ $n \cdot cm^{-2} \cdot s^{-1} \cdot eV^{-1}$

$b = 0.983 \pm 0.0004$

MADAP are given in Table 5 and the spectrum is shown in Fig. 3. The corresponding measured saturation activities and the ratios of calculated and measured activities are shown is Tables 6 and 7.

Comparison to LOUHI78

For comparison, the fast neutron spectrum was also unfolded with the program LOUHI78.[4] For numerical solution the activation Eqs. (1) are expressed in discrete matrix form

$$\underline{A} = \underline{K}\,\underline{\sigma} + \underline{\epsilon}, \tag{52}$$

where $\underline{A}$ – vector of k saturation activities,
$\underline{\phi}$ – vector of flux values at n energy points,
$\underline{K}$ – k x n response matrix constructed with activation cross-sections,
$\underline{\epsilon}$ – unknown error vector of $\underline{A}$.

Table 6
Saturation activities A_i^m of the components of a resonance MAD used to measure the intermediate spectrum in Triga reactor, Fig. 3, and ratios of calculated and measured activities (A_i^c/A_i^m)

Reaction	A_i^m, dec/s	A_i^c/A_i^m
^{115}In (n, γ) ^{116m}In	$5.01 \cdot 10^{-10}$	1.03
^{197}Au (n, γ) ^{198}Au	$3.54 \cdot 10^{-10}$	0.92
^{186}W (n, γ) ^{187}W	$1.06 \cdot 10^{-10}$	1.04
^{75}As (n, γ) ^{76}As	$1.29 \cdot 10^{-11}$	1.06
^{198}Pt (n, γ) ^{199}Pt	$8.99 \cdot 10^{-12}$	1.22
^{55}Mn (n, γ) ^{56}Mn	$3.17 \cdot 10^{-12}$	1.09
^{63}Cu (n, γ) ^{64}Cu	$1.28 \cdot 10^{-12}$	0.91
^{23}Na (n, γ) ^{24}Na	$7.62 \cdot 10^{-14}$	0.86

Table 7
Saturation activities A_i^m of the components of a threshold MAD used to measure the fast spectrum in Triga reactor, Figs. 3 and 4, and the ratios of calculated and measured saturation activities (A_i^c/A_i^m) as given by the fission spectrum fitting program MADAP and by the unfolding program LOUHI78

Reaction	A_i^m, dec/s	A_i^c/A_i^m	
		MADAP	LOUHI78
^{27}Al (n, α) ^{24}Na	$6.75 \cdot 10^{-16}$	1.09	1.06
^{46}Ti (n, p) ^{46}Sc	$1.06 \cdot 10^{-14}$	1.09	1.03
^{47}Ti (n, p) ^{47}Sc	$1.66 \cdot 10^{-14}$	1.02	1.05
^{48}Ti (n, p) ^{48}Sc	$3.03 \cdot 10^{-16}$	0.85	0.88
^{54}Fe (n, p) ^{54}Mn	$7.97 \cdot 10^{-14}$	0.96	0.94
^{56}Fe (n, p) ^{56}Mn	$1.04 \cdot 10^{-15}$	1.11	1.03
^{58}Ni (n, p) ^{58}Co	$1.07 \cdot 10^{-13}$	0.96	0.96
^{93}Nb (n, 2n) ^{92m}Nb	$4.89 \cdot 10^{-16}$	0.77	1.02
^{115}In (n, n') ^{115m}In	$2.02 \cdot 10^{-13}$	0.89	1.00

In practice n is larger than k and Eq. (52) is underdetermined and a priori knowledge of the spectrum is used to get a physically acceptable solution. In the nonlinear method of LOUHI78 the nonnegativity of the spectrum is guaranteed by expressing the flux values as squares of real numbers

$$\phi_j = X_j^2, j = 1, ..., n. \quad (53)$$

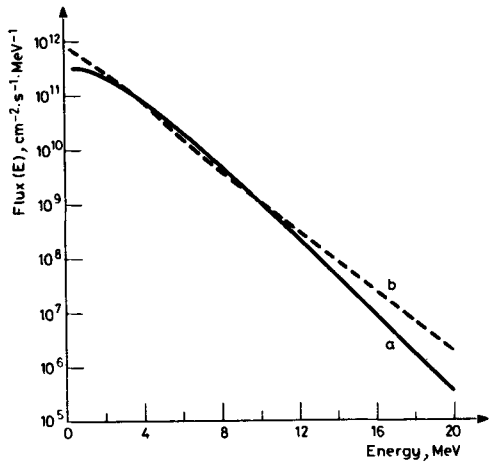

Fig. 4. Fast neutron flux spectrum in Triga. a) Fission spectrum fitted with the program MADAP, b) spectrum unfolded with LOUHI78. The corresponding activities are given in Table 7

To implement other prior conditions Eq. (52) is transformed into the minimization problem

$$\min Q = Q_0 + \gamma \sum_{\ell=1}^{5} Q_\ell , \tag{54}$$

where

$$Q_0 = \sum_{i=1}^{k} \frac{\epsilon_i^2}{A_i^2} = \sum_{i=1}^{k} \frac{1}{A^2{}_i} \left(A_i - \sum_{j=1}^{n} K_{ij} X_j{}^2\right)^2 , \tag{55}$$

is the square sum of relative fitting errors of the activities. The terms Q_1, ..., Q_5 are related to the assumed shape and smoothness of the spectrum and the regularization parameter γ determines the weight of the prior conditions.

In this work only the prior condition Q_4 of Ref.[4] was used in the form

$$Q_4 = \sum_{j=2}^{n-1} \frac{1}{n} (\log X_{j-1}{}^2 - 2 \log X_j{}^2 + \log X_{j+1}{}^2)^2 , \tag{56}$$

which imposes a smoothness condition by minimizing the square sum of the second differences of the logarithm of the solution. The nonlinear minimization of Eq. (54) is carried out with an iterative gradient type algorithm with a variable metric.

In Fig. 4 the fast neutron spectrum is shown both as unfolded with LOUHI78 and as fitted with MADAP. The corresponding ratios of calculated and measured activities are given in Table 7.

Some deviations can be seen between the unfolded and fitted spectra at the ends of the energy scale. This can be easily understood as activation detectors have poor resolution in these energy regions and the spectrum is defined by the a priori conditions, which are different for the two methods. It is difficult to say whether the differences in the spectra are real or they are caused by measuring and cross-section errors, since the agreement of the measured and calculated activities is fairly good for both methods. The average fitting error of activities was 9.7% for the fission spectrum and 4.6% for LOUHI78.

Conclusions

The functional fitting procedure has been shown to give satisfactory results for the Triga reactor spectrum in the energy regions covered by the multicomponent detectors. The method can be used in such applications as, e.g., the determination of spectra to evaluate epithermal contribution in activation analysis.

The use of the funcitonal fitting method is justified by the simplicity of the computations and by the easy interpretation of the results. If a good fit of the measured activities cannot be reached by the simple method, the user can resort to more sophisticated unfolding programs such as LOUHI78, SAND–II or STAY'SL.

In the energy region of 0.1 – 1.5 MeV the functional representation is not very reliable, since the spectrum is neither a C/E^n nor a fission spectrum. This is not a serious disadvantage for the fitting method, since neither resonance nor threshold detectors are sensitive in this interval. If knowledge of this interval is essential, fission detectors can be used and the functional fitting method can be improved with a joining function which links smoothly the C/E^n and fission spectra.

*

The help and collaboration of Prof. J. T. ROUTTI, Dr. M. J. KOSKELO and Mr. P. A. AARNIO is gratefully acknowledged.

References

1. P. A. AARNIO, M. J. KOSKELO, P. D. LUND, V. K. MAUNULA, J. T. ROUTTI, J. V. SANDBERG, H. J. TAKALA, Nuclear Technology 58 (1982) 318
2. M. J. KOSKELO, J. T. ROUTTI, H. TAKALA, Multicomponent Resonance and Threshold Detectors for Reactor Neutron Spectroscopy and Damage Studies, in the Proc. of the Third ASTM-EURATOM Conference on Radiation Damage, Ispra (Varese) 1979, Report EUR 6813 EN-FR, 1980.
3. P. A. AARNIO, M. J. KOSKELO, Nuclear Technology, 59 (1982) 170.
4. J. T. ROUTTI, J. V. SANDBERG, Comput. Phys. Commun., 21 (1980) 119.
5. W. N. McELROY et al., A Computer Automated Iterative Method for Neutron Flux Spectra Determination by Foil Activation, Vol. I–IV, U. S. Air Force Weapons Laboratory Report AFWL–TR–67–41, 1967.

6. F. G. PEREY, Least-Squares Dosimetry Unfolding: The Program STAY'SL, Oak Ridge National Laboratory Report ORNL/TM–6062, 1977.
7. P. D. LUND, J. V. SANDBERG, Direct Computation of Neutron Spectra from Multicomponent Activation Detectors, Helsinki University of Technology Report TKK–F–A409, 1980.
8. M. J. KOSKELO, P. A. AARNIO, J. T. ROUTTI, Comput. Phys. Commun., 24 (1981) 11.
9. G. ERDTMANN, Neutron Activation Tables, Verlag Chemie, Weinheim, 1976.
10. K. H. BECKURTS, K. WIRTZ, Neutron Physics, Springer Verlag, Berlin, 1964.
11. K. M. CASE, F. de HOFFMANN, G. PLAZEK, Introduction to the Theory of Neutron Diffusion, Vol. I, Los Alamos Scientific Laboratory, NM, 1953.
12. Engineering Compendium on Radiation Shielding, Vol. I, Springer Verlag, Berlin-Heidelberg, 1975.
13. H.–L. PAI, P.–Y. MA, W. S. LEE, Nucl. Sci. Eng., 9 (1961) 519.
14. Neutron Fluence Measurements, IAEA Technical Reports Series no 107, Vienna, 1970.
15. B. W. RUST, W. R. BURRUS, Mathematical Programming and the Numerical Solution of Linear Equations, American Elsevier, New York, 1972.
16. W. T. EADIE, D. DRIJARD, F. E. JAMES, M. ROOS, B. SADOULET, Statistical Methods in Experimental Physics, North Holland Publishing Co., Amsterdam, 1971.
17. B. E. WATT, Phys. Rev., 87 (1951) 1037.
18. E. C. CRAMER, Mathematical Methods of Statistics, Princeton, NJ., 1946.
19. W. L. ZIJP et al., Compilation of Evaluated Cross Section Data Used in Fast Neutron Metrology, Reactor Centrum Nederland, Petten, Report RCN–196, 1973.
20. G. ERDTMANN, W. SOYKA, Die γ-Linien der Radionuklide, Band 1, KFA Jülich Report Jül–1003–AC, 1973.
21. C. MEIXNER, Gammaenergien, Teil I, KFA Jülich Report Jül–1087–RX, 1974.